



저작자표시-비영리-변경금지 2.0 대한민국

이용자는 아래의 조건을 따르는 경우에 한하여 자유롭게

- 이 저작물을 복제, 배포, 전송, 전시, 공연 및 방송할 수 있습니다.

다음과 같은 조건을 따라야 합니다:



저작자표시. 귀하는 원저작자를 표시하여야 합니다.



비영리. 귀하는 이 저작물을 영리 목적으로 이용할 수 없습니다.



변경금지. 귀하는 이 저작물을 개작, 변형 또는 가공할 수 없습니다.

- 귀하는, 이 저작물의 재이용이나 배포의 경우, 이 저작물에 적용된 이용허락조건을 명확하게 나타내어야 합니다.
- 저작권자로부터 별도의 허가를 받으면 이러한 조건들은 적용되지 않습니다.

저작권법에 따른 이용자의 권리는 위의 내용에 의하여 영향을 받지 않습니다.

이것은 [이용허락규약\(Legal Code\)](#)을 이해하기 쉽게 요약한 것입니다.

[Disclaimer](#)

Master's Thesis
석사 학위논문

A Chemical Route to Activation of Open Metal Sites in
the Copper-Based Metal–Organic Framework Materials
HKUST-1 and Cu-MOF-2

Hong Ki Kim (김 홍 기 金 洪 基)

Department of Emerging Materials Science

신물질과학전공

DGIST

2016

Master's Thesis
석사 학위논문

A Chemical Route to Activation of Open Metal Sites in
the Copper-Based Metal–Organic Framework Materials
HKUST-1 and Cu-MOF-2

Hong Ki Kim (김 홍 기 金 洪 基)

Department of Emerging Materials Science

신물질과학전공

DGIST

2016

A Chemical Route to Activation of Open Metal Sites in
the Copper-Based Metal–Organic Framework Materials
HKUST-1 and Cu-MOF-2

Advisor: Professor Nak Cheon Jeong
Co-advisor: Professor Jong-Soo Lee

By

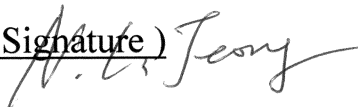
Hong Ki Kim
Department of Emerging Materials Science
DGIST

A thesis submitted to the faculty of DGIST in partial fulfillment of the requirements for the degree of Master of Science in the Department of Emerging Material Science. The study was conducted in accordance with Code of Research Ethics¹

7. 6. 2016

Approved by

Professor Nak Cheon Jeong
(Advisor)

(Signature) 

Professor Jong-Soo Lee
(Co-Advisor)

(Signature) 


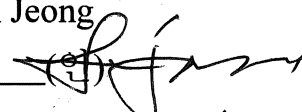

¹ Declaration of Ethical Conduct in Research: I, as a graduate student of DGIST, hereby declare that I have not committed any acts that may damage the credibility of my research. These include, but are not limited to: falsification, thesis written by someone else, distortion of research findings or plagiarism. I affirm that my thesis contains honest conclusions based on my own careful research under the guidance of my thesis advisor.

A Chemical Route to Activation of Open Metal Sites in
the Copper-Based Metal–Organic Framework Materials
HKUST-1 and Cu-MOF-2

Hong Ki Kim

Accepted in partial fulfillment of the requirements for the degree of Master of
Science.

7. 6. 2016

Head of Committee 정낙천 (인) 
Prof. Nak Cheon Jeong
Committee Member 이종수 (인) 
Prof. Jong-Soo Lee
Committee Member 이재동 (인) 
Prof. JaeDong Lee

MS/EM
201441003

김 흥 기. Hong Ki Kim. A Chemical Route to Activation of Open Metal Sites in the Copper-Based Metal–Organic Framework Materials HKUST-1 and Cu-MOF-2. Department of Emerging Materials Science. 2016. 50p. Advisors Prof. Nak Cheon Jeong, Co-Advisors Prof. Jong-Soo Lee.

Abstract

Open coordination sites (OCSs) in metal–organic frameworks (MOFs) often function as key factors in the potential applications of MOFs, such as gas separation, gas sorption, and catalysis. For these applications, the activation process to remove the solvent molecules coordinated at the OCSs is an essential step that must be performed prior to use of the MOFs. To date, the thermal method performed by applying heat and vacuum has been the only method for such activation. In this report, we demonstrate that methylene chloride (MC) itself can perform the activation role: this process can serve as an alternative “chemical route” for the activation that does not require applying heat. To the best of our knowledge, no previous study has demonstrated this function of MC, although MC has been popularly used in the pretreatment step prior to the thermal activation process. On the basis of a Raman study, we propose a plausible mechanism for the chemical activation, in which the function of MC is possibly due to its coordination with the Cu^{2+} center and subsequent spontaneous decoordination. Using HKUST-1 film, we further demonstrate that this chemical activation route is highly suitable for activating large-area MOF films.

Keywords: Metal-organic frameworks (MOFs), Open coordination sites (OCSs), Methylene chloride (MC), Activation

Contents

Abstract	i
Contents	ii
List of tables	iv
List of figures	v
I. INTRODUCTION	1
1.1 Metal-Organic Frameworks (MOFs)	1
1.2 Analyzation for Structural frame of HKUST-1	2
1.3 Open Coordination Sites (OCSs)	3
1.4 Present Strategies for Activation of Open Coordination Sites (OCSs)	5
1.5 Motivation and Purpose	6
II. EXPERIMENTAL DETAILS	8
2.1 Material and methods.....	8
2.1.1 Materials	8
2.1.2 Synthesis of HKUST-1.....	9
2.1.3 Synthesis of Cu-MOF-2.....	9
2.1.4 Synthesis of HKUST-1film on patterned copper plate. .	10
2.1.5 Thermal activation (TA) of HKUST-1 and Cu-MOF-2. .	11
2.1.6 Chemical activation (CA) of HKUST-1 and Cu-MOF-211	
2.1.7 Exchange of coordinated molecules in HKUST-1	12
2.1.8 Sample preparation for the Raman and UV-vis absorption	
analysis.....	12
2.1.9 Sample preparation for the ¹ H-NMR measurements	13
2.1.10 Sample preparation for measurement of moisture	
sorption.....	13

2.2 Instrumentation	13
III. RESULTS AND DISCUSSION.....	15
1.1 Optical Color Change between Pristine HKUST-1 and Treated HKUST-1	15
1.2 Structural Stability and Molecules Dissociation of Thermally Treated HKUST-1	16
1.3 Structural stability and Surface Areas of Treated HKUST-1	17
1.4 ¹ H-NMR, Raman, and BET Results for Room Temperature Evacuation of HKUST-1	20
1.5 The Surest Evidence of Molecules Dissociation for MC treated HKUST- 1	21
1.6 Raman Spectra and Water sorption Experiments of HKUST-1	23
1.7 Raman Spectra of Activated HKUST-1 after Exposure to Ambient Atmosphere	28
1.8 Theoretical Studies for Raman Shift of Cu-Cu vibration in HKUST-1 .	29
1.9 ¹ H-NMR, Raman and BET Result for Room Temperature Evacuation of HKUST-1	32
1.10 Application to Cu-MOF-2 with Chemical Activation	33
1.11 Structural Stability of Treated Cu-MOF-2.....	36
1.12 Application to Large size MOF Films with Chemical Activation....	36
IV. CONCLUSION	38
V. REFERENCE.....	39

List of tables

Table I. Bond Length ($d_{\text{Cu-Cu}}$) and Stretching Vibration Frequency ($\nu_{\text{Cu-Cu}}$) of Cu-Cu Bonding in HKUST-1.....	32
--	----

List of figures

- Figure 1. A representative metal-organic framework material: $\text{Cu}_3(\text{BTC})_2$ (HKUST-1). Blue, gray, red spheres and green poles represent Cu, C, O atoms and open coordination sites, respectively; H atoms have been omitted for clarity. 1
- Figure 2. Illustration of cages and windows within HKUST-1 and 2-dimensional representation of the topological arrangements of the cages. Hydrogen atoms bonded to carbon in BTC are omitted for the sake of clarity. 3
- Figure 3. Schematic illustration of chemical activation of the paddle-wheel-like $(\text{Cu}^{\text{II}})_2$ node within HKUST-1 or Cu-MOF-2 performed by MC. Hydrogen atoms bound to carbon atoms in the benzene moieties are omitted for the sake of clarity. 7
- Figure 4. Diffuse reflectance UV-vis absorption spectra of pristine-HK (black curve), TA-HK (red curve), and MC-HK (blue curve) crystalline powders. The circular insets show optical microscope images of the samples as indicated. 15
- Figure 5. (a) ^1H -NMR spectra and (b) PXRD patterns of pristine-HK and TA-HK powder samples. The TA was performed at 150 °C for 12 h. The NMR spectra were taken after completely dissolving the powder samples in

D ₂ SO ₄	17
Figure 6. PXRD patterns of pristine-, EtOH-, MeOH-, and MeCN-coordinated HKUST-1 (a) before and (b) after MC treatment.	18
Figure 7. N ₂ adsorption/desorption isotherms of TA-HK and MC-HK powders, as indicated.....	19
Figure 8. (a) ¹ H-NMR and (b) Raman spectra of pristine-HK sample after applying only vacuum at room temperature for 2 h. The NMR spectrum was taken after completely dissolving the powder samples in D ₂ SO ₄ .21	
Figure 9. ¹ H-NMR spectra of pristine-, EtOH-, MeOH-, and MeCN-coordinated HKUST-1 (a) before and (b) after MC treatment. The NMR spectra were taken after completely dissolving the powder samples in D ₂ SO ₄	23
Figure 10. Raman spectra of MC, ethanol (EtOH), and water (H ₂ O), as indicated.	25
Figure 11. (a) Illustration of H ₂ O-coordinated, CH ₂ Cl ₂ -coordinated, and ligand-free (Cu ^{II}) ₂ centers. (b) Expanded (left panel) and wide (right panel) views of Raman spectra obtained from bare quartz container (gray curve), pristine-HK (black curve), TA-HK (red curve), HK wet in MC (pink curve), and dry MC-HK (blue curve) samples. (c) Plots of increase in the weights of the TA-HK and MC-HK samples with respect to the exposure time to ambient atmosphere (approximately	

30% relative humidity). The inset shows the weight change of the MC-HK sample in the initial exposure. (d) Expanded (left panel) and wide (right panel) views of the spectral changes in the Raman shifts of a dry MC-HK sample according to the exposure time to ambient atmosphere in intervals of 3 min [i.e., after (i) 0, (ii) 3, (iii) 6, (iv) 9, (v) 12, (vi) 15, and (vii) 18 min]. 27

Figure 12. Raman spectra of pristine-HK, TA-HK, and MC-HK powder samples taken after exposure to ambient atmosphere for 2 h. We employed a crystalline silicon substrate for the powder sample in order to utilize the substrate as an internal standard. 28

Figure 13. Raman spectra of MC, ethanol (EtOH), and water (H₂O), as indicated. 31

Figure 14. (a) ¹H-NMR and (b) Raman spectra of pristine-HK sample after applying only vacuum at room temperature for 2 h. The NMR spectrum was taken after completely dissolving the powder samples in D₂SO₄.33

Figure 15. N₂ adsorption isotherms of a pristine-HK sample after applying only vacuum at room temperature for 2 h. We could not obtain a complete data set from BET due to the acquisition time limit of the equipment.33

Figure 16. (a) Diffuse reflectance UV-vis absorption spectra of pristine-MOF-2 (black curve), TA-MOF-2 (red curve), and MC-MOF-2 (blue curve) crystalline powders. The optical microscope images in the circular

insets display the colors of the powder samples. (b) $^1\text{H-NMR}$ spectra of pristine-MOF-2, TA-MOF-2, and MC-MOF-2 taken after the samples were dissolved in D_2SO_4 . (c) Expanded (left panel) and wide (right panel) views of the Raman spectra of pristine-, TA-, and MC-MOF-2 powder samples. The Raman spectra were taken after the samples were sealed in a moisture-free argon-charged glove box. 35

Figure 17. PXRD patterns of pristine-MOF-2, TA-MOF-2, and MC-MOF-2 powder samples, as indicated. 36

Figure 18. Photographs of the (a) patterned Cu substrate, (b) surface-oxidized Cu substrate ($\text{Cu}_2\text{O}/\text{Cu}$), (c) pristine HKUST-1 film synthesized on the Cu substrate, and (d) MC-treated HKUST-1 film. $^1\text{H-NMR}$ spectra of (e) pristine- and (f) MC-treated HKUST-1 films. XRD patterns of (e) pristine- and (f) MC-treated HKUST-1 films. 37

I. INTRODUCTION

1.1 Metal-Organic Frameworks (MOFs)

Metal-organic frameworks (MOFs), which are assembled by an alternating interconnection of inorganic components (either metal ions or metal oxide clusters) with multitopic organic ligands (as linkers) have emerged as a distinguished class of nanoporous crystalline materials with ultrahigh porosity and enormous internal and external surface areas.¹⁻⁷

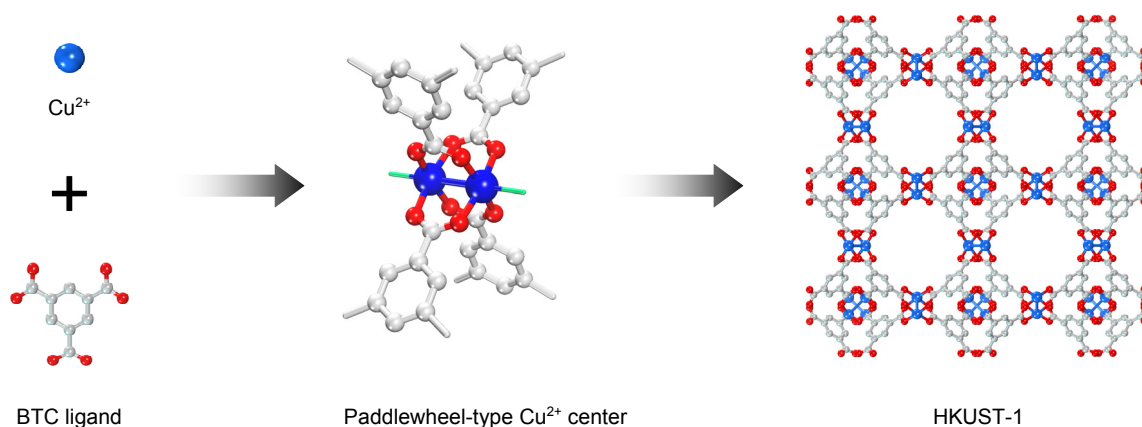


Figure 1. A representative metal-organic framework material: $\text{Cu}_3(\text{BTC})_2$ (HKUST-1). Blue, gray, red spheres and green poles represent Cu, C, O atoms and open coordination sites, respectively; H atoms have been omitted for clarity.

Lately, MOFs on a fundamental standard represent the artistic regularity of chemical building structures and the valuable materials with combining organic and inorganic chemistry. The features with the extraordinary degree of diversity for both the organic and inorganic components in their structures, make MOFs of interest for various potential applications. Notably, on top of their extraordinarily high surface areas, MOFs are known for various catalytic properties, tunable pore size and adjustable internal surface properties through changing or functionalizing metal or ligand components.

1.2 Analyzation for Structural frame of HKUST-1

HKUST-1 has three types of cages and two types of windows (see **Figure 2**).²³ Three-dimensional type 1 and type 2 large cages are alternately interconnected and share large windows (see **Figures 2d and 2f**). The small cages (type 3) formed at the edges of large cages share small windows with type 2 large cages (see **Figures 2e and 2f**). The sizes of the windows are presented in **Figures 2d and 2e**. All of the axial OCSs on the $(\text{Cu}^{\text{II}})_2$ centers face the type 1 large cages such that free ligands (i.e., solvents) can be easily accessed. Regarding its structure, alternative face centered cubic (fcc) close packing of the type 1 and type 2 cages constructs HKUST-1. Whereas the small cages (type 3) formed at the edges of the large cages preclude free access of guest molecules because of aperture blockage by the benzene moiety in BTC, the large cages allow fast access to guests through their large open spaces. What is notable is that all OCSs face toward the open spaces of the large cages (type

1).

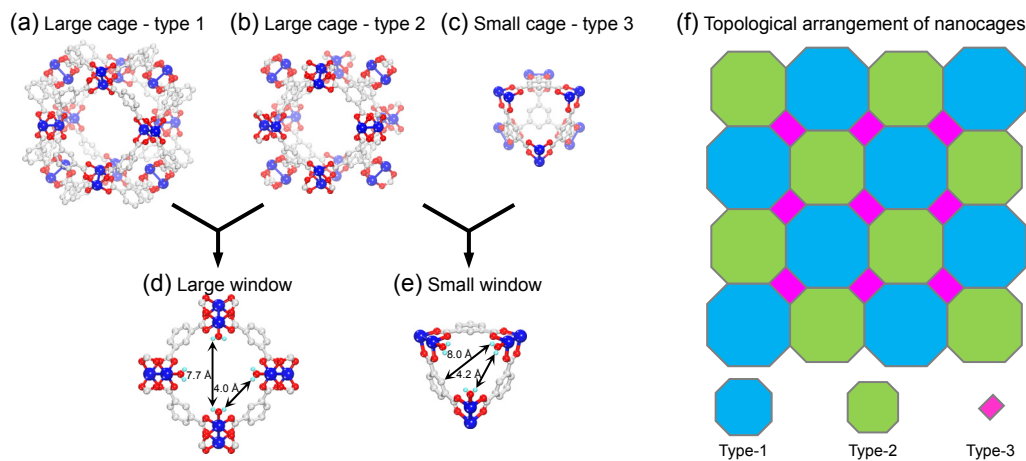


Figure 2. Illustration of cages and windows within HKUST-1 and 2-dimensional representation of the topological arrangements of the cages. Hydrogen atoms bonded to carbon in BTC are omitted for the sake of clarity.

1.3 Open Coordination Sites (OCSs)

Porous materials is deserved to be explored although it is unprecedented. Most of all, the dynamics of molecules within MOF structures is an important topic that can lead to better designs for open coordination sites MOFs. In principle, the MOFs with OCSs that can be obtained, and they might be able to activate the small molecules such as H₂O, CO, CO₂, etc., subsequently trigger their chemical reactions under mild conditions (see **Figure 1**). This fact thus makes HKUST-1 more valuable because guest molecules can be more readily accessible to the OCS, and the molecules decoordinated from the OCS can be easily removed through the large open spaces. In addition, HKUST-1 has the ability to replace its

precoordinated solvent (EtOH, MeOH, MeCN, etc.) with other Lewis base polar guest molecules when the Lewis base molecules are sufficiently fed.

Namely, MOF materials have pores decorated with open metal sites at the pore surface. Particularly, in metal-organic framework material, open coordination sites (OCSs), coordinatively vacatable sites at the metal center (typically where Lewis base (LB) molecules can ligate with weak coordination bonding to be reversibly dissociable), have been demonstrated to play an important role in potential applications of MOFs, such as chemical separation,⁸⁻¹⁰ gas storage,^{8,11-18} heterogeneous catalysis,^{8,19-21} sensing,²² and ion conduction,^{8,23-24} among others.²⁵⁻²⁶ HKUST-1, an MOF that is constructed of multiple links of paddle-wheel-like coordination between two Cu^{2+} ions and four 1,3,5-benzenetricarboxylate (BTC) linkers (see **Figure 1**), is a good example of an MOF that possesses a very high concentration of OCSs.²⁷ A feature of HKUST-1 is that two types of large cages are three-dimensionally interconnected in an alternating fashion with a face-centered cubic topology. Another good example of an OCS-containing MOF is the MOF-2 series, which comprises transition metal ions such as Cu^{2+} or Zn^{2+} and 1,4-benzenedicarboxylate (BDC) linkers. The coordination mode in MOF-2 is same as the coordination mode in HKUST-1. However, in contrast to HKUST-1, the architecture of MOF-2 is based on stacking lamellar phase sheets of $\text{Cu}_2(\text{BDC})_2$ in two dimensions. The “extracoordination” (solvent coordination) ability of the OCSs in both HKUST-1 Preceding researches and MOF-2 enables them to be excellent adsorbents or molecule separators for applications such as carbon dioxide sorption,^{11,28-29} water sorption,³⁰ amine sorption,³¹ nitric

oxide capture,³² water/ethanol separation,³³ and others.^{9,19–20,22–24,34–36}

1.4 Present Strategies for Activation of Open Coordination Sites (OCSs)

To utilize that type of MOF for the aforementioned applications, an activation process to remove both pre-coordinating solvent molecules from the OCS and pore-filling guest molecules (typically the solvents used during the synthesis process) from the pores is a prerequisite step.³⁷ To date, five strategies³⁸ for effective activation have been developed: (i) thermal activation (by applying heat and vacuum; hereafter TA),^{39–43} (ii) solvent exchange (typically performed by methylene chloride or chloroform),^{44–45} (iii) freeze-drying,⁴⁶ (iv) supercritical CO₂ exchange,⁴⁵ and (v) chemical treatment (typically with HCl only in the cases where corresponding MOFs are exceptionally stable in strong acidic environment, for examples, MOFs constructed with zirconium oxide cluster such as PCN-222 (also known as MOF-545) and NU-1000).^{21,25,47} Among these strategies, TA has been most commonly used because it can completely remove pore-filling solvents and it is the only known method that can remove components of both coordinated and pore-filling solvents. However, often characterized by TA's negative influence on structural integrity,^{37,45,48–49} the TA process has evolved by combining it with the solvent exchange method because employment of a solvent with a lower boiling point, e.g., methylene chloride (CH₂Cl₂, hereafter MC) or chloroform (CHCl₃), can aid in lowering the activation temperature and thereby minimizing the potential structural damage. Yaghi and co-workers first demonstrated that treatment with chloroform prior to TA is quite effective for complete removal of the pore-filling solvent under mild

conditions.⁴⁴ However, it is surprising that although such solvents (e.g., CH₂Cl₂ or CHCl₃) have frequently been used in solvent exchange processes to support permanent porosity by removing pore-filling solvents, to the best of our knowledge, there has been no systematic study of their secondary function, i.e., scissoring the solvent coordination at the OCS.

1.5 Motivation and Purpose

As mentioned above, we questioned whether even MC can be substituted by exchanging the precoordinated H₂O and EtOH (solvents used in synthesis) in pristine HKUST-1, although the polarity of MC is much less, considering the primitive assumption that the MC is also a weak Lewis base that possesses lone-paired electrons in its chlorine atoms.⁵⁰⁻⁵⁴ Our postulate was that if the MC molecules can be replaced, the coordination of MC will be substantially more than sufficiently labile to be spontaneously dissociated with a low activation energy (thermal energy at room temperature). If it is so labile, then MC treatment itself in the absence of supplied heat can be an effective, cost-effective chemical method for activation of OCSs.

Furthermore, we demonstrate that this chemical activation process is highly useful for activating large-area films, which is likely to be costly and cumbersome due to the requirement of massive equipment for applying heat and vacuum when the conventional thermal method is used for the activation.³⁷ Also, we suggest a plausible mechanism for this “chemical activation” route on the basis of Raman studies. Here, we report regarding the scissoring function of MC. Although several MOFs that possess OCSs should be suitable for

this demonstration, we limited our studies to HKUST-1 and Cu-MOF-2. As described below, we found that soaking HKUST-1 or MOF-2 in fresh MC for only 5 min at room temperature and subsequent repetition of the process several times led to decoordination of the H₂O, EtOH, MeOH, MeCN, and even dimethylformamide (DMF) bound to the OCSs (see **Figure 3**).

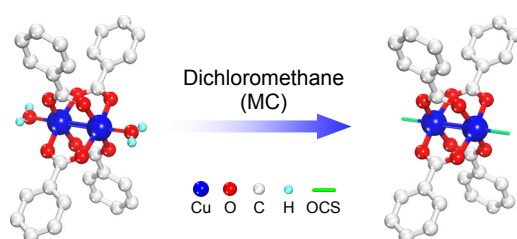


Figure 3. Schematic illustration of chemical activation of the paddle-wheel-like $(\text{Cu}^{\text{II}})_2$ node within HKUST-1 or Cu-MOF-2 performed by MC. Hydrogen atoms bound to carbon atoms in the benzene moieties are omitted for the sake of clarity.

II. EXPERIMENTAL DETAILS

2.1 Material and methods

2.1.1 Materials

All reagents were obtained from commercial sources (Sigma Aldrich, Alfa Aesar, or Daejung) and were used without further purification. Copper (II) nitrate [$\text{Cu}(\text{NO}_3)_2 \cdot 3\text{H}_2\text{O}$, 98.0-103%, Aldrich], trimesic acid (1,3,5-benzenetricarboxylic acid, BTC, 95%, Aldrich), ethanol (EtOH, 96%, Daejung), N,N-Dimethylformamide (DMF, 99.8%, Aldrich), and distilled deionized water (DDW) were used for synthesis of HKUST-1 in both the crystalline powder and film forms. 1,4-Benzenedicarboxylic acid (BDC, 98+%, Alfa Aesar) was used with copper (II) nitrate for synthesis of Cu-MOF-2 powder. Methylene chloride (CH_2Cl_2 , MC, 99.5%, Aldrich) was employed as a reagent for chemical activation (CA). Anhydrous methanol (MeOH, 99.8%, Aldrich), anhydrous ethanol (EtOH, 99.5%, Aldrich), and anhydrous acetonitrile (MeCN, 99.8%, Aldrich) were employed for substitution of pre-coordinated water and ethanol in pristine HKUST-1. Sulfuric acid-d₂ (D_2SO_4 , 96-98 wt% in D_2O , 99.5 atomic % in deuterium, Aldrich) was used for dissolving HKUST-1 and Cu-MOF-2 prior to performing ¹H-NMR spectroscopy on the samples. Copper-clad laminate board (RS component code: 159–5773) was used for making printed circuit boards (PCBs), which were used as the substrate for the HKUST-1 film, and ammonium persulfate [$(\text{NH}_4)_2\text{S}_2\text{O}_8$, 98%, Aldrich] was used for oxidizing metallic copper prior to synthesis of the HKUST-1 film. All

synthesized MOF powders and films were stored in a moisture-free argon-charged glove box prior to use.

2.1.2 Synthesis of HKUST-1

We synthesized HKUST-1 following the procedure described in a previous report.²³ Briefly, $\text{Cu}(\text{NO}_3)_2 \cdot 3\text{H}_2\text{O}$ (0.87 g, 3.6 mmol) was dissolved in 10 mL of DDW in a vial. In a separate vial, BTC (0.22 g, 1.0 mmole) was dissolved in 10 mL of EtOH. The $\text{Cu}(\text{NO}_3)_2$ solution was quickly added into the vial in which the BTC solution was contained. After continuous stirring for 10 min at room temperature, 1 mL of DMF was added to the mixed solution. Then, the vial was sealed with polytetrafluoroethylene (PTFE) tape. The vial was placed in an oven at 80 °C for 20 h to allow the mixture to react. After allowing the product to cool to room temperature, we collected and washed the crystalline solid (pristine HKUST-1) with H_2O and EtOH.

2.1.3 Synthesis of Cu-MOF-2

We also synthesized Cu-MOF-2 following the procedure described in previous reports.⁵⁵⁻⁵⁷ $\text{Cu}(\text{NO}_3)_2 \cdot 3\text{H}_2\text{O}$ (0.242 g, 1.0 mmol) was dissolved in 10 mL of DMF in a vial. In a separate vial, BDC (0.166 g, 1.0 mmol) was dissolved in 10 mL of DMF. The $\text{Cu}(\text{NO}_3)_2$ solution was quickly added to the BDC solution. After continuous stirring for 10 min at room

temperature, the vial was sealed with PTFE tape. Then, the vial was placed in an oven at 110 °C for 48 h to allow the mixture to react. After allowing the vial to cool to room temperature, we collected and washed the crystalline solid (pristine Cu-MOF-2) with fresh DMF.

2.1.4 Synthesis of HKUST-1 film on patterned copper plate.

HKUST-1 films were synthesized on patterned copper-clad laminate plate. First, the copper-clad plates were patterned using the routine photolithography method. Then, the metallic copper surface was smoothed using a polisher and alumina powder, and the plate was washed with acetone and ethanol. The washed copper plate was put into 2 wt% $(\text{NH}_4)_2\text{S}_2\text{O}_8/\text{DDW}$ solution and then allowed to oxidize for 30 s. After washing with DDW, the plate was placed into a plastic box in which 150 mM BTC solution of mixed H_2O and EtOH solvent were contained. Then, the copper substrate was allowed to react with the BTC at 40 °C for 7 d. Subsequently, the HKUST-1 film that was formed was washed with copious amounts of fresh EtOH. Then, the film was transferred into a moisture-free Ar-charged glove box prior to use.

2.1.5 Thermal activation (TA) of HKUST-1 and Cu-MOF-2

Coordinated solvents in pristine HKUST-1 (H₂O and EtOH) and Cu-MOF-2 (DMF) were removed by TA. For this TA, pristine HKUST-1 powder was placed into a glass vacuum tube. Then, the tube was heated at 150 °C for 12 h under vacuum ($\sim 10^{-3}$ torr). The method for the TA of Cu-MOF-2 powder was the same as the above procedure except for the activation temperature, which was approximately 200 °C. After activation, the tubes were transferred into an Ar-charged glove box prior to use.

2.1.6 Chemical activation (CA) of HKUST-1 and Cu-MOF-2

0.05 g of pristine HKUST-1 powder were placed into 20 mL of MC. Then, the pre-coordinated H₂O and EtOH were removed for 5 min. This process was repeated 5 times to successfully activate the HKUST-1. The process for the chemical activation of Cu-MOF-2 was same as the above procedure except for the number of repetitions of the procedure (12 times). In the case of the HKUST-1 films, the process was achieved by dipping the films into fresh MC solvent for 5 min. This procedure was also repeated 5 times. The entire chemical activation process was performed in a moisture-free argon-charged glove box.

2.1.7 Exchange of coordinated molecules in HKUST-1

The substitution of pre-coordinated solvent molecules in pristine HKUST-1 (H₂O and EtOH) was performed following the procedure described in a previous report.²³ Briefly, thermally activated HKUST-1 powder samples were placed in vials, and methanol (MeOH) was put into the vial. Then, the activated HKUST-1 was allowed to react with the methanol for 1 h. Subsequently, the MeOH-coordinated HKUST-1 (MeOH-HK) that was formed was collected by filtration and dried under an Ar atmosphere before use. Substitution by ethanol (EtOH) and acetonitrile (MeCN) was achieved using the same procedure. All of the processes were conducted under an inert atmosphere in a moisture-free argon-charged glove box.

2.1.8 Sample preparation for the Raman and UV-vis absorption analysis

Prior to taking Raman and UV-vis absorption spectra, HKUST-1 or Cu-MOF-2 powder samples were contained in cylindrical quartz cells (Starna, Type 37GS Cylindrical Cells with Quartz to Borofloat graded seal). The preparation was performed in a moisture-free Ar-charged glove box, and the cells were sealed with a glass cork using a grease (Apiezon, H high temperature Vacuum Greases) prior to the measurements.

2.1.9 Sample preparation for the ^1H -NMR measurements

A tiny amount of HKUST-1 or Cu-MOF-2 powder was dissolved in 1 mL of D_2SO_4 . Then, the solution was transferred into an NMR tube. This preparation was also conducted in an Ar-charged glove box. Additionally, the tubes were sealed with plastic caps and acrylic Parafilm[®] prior to being removed from the glove box.

2.1.10 Sample preparation for measurement of moisture sorption

To check moisture sorption of thermally activated HKUST-1 (TA-HK), the powder sample (~100 mg) was spread onto a light, shallow plastic container (4 cm \times 4 cm) placed on top of a microbalance, and the initial weight of the powder was quickly measured. Then, the increase in the weight of the powder was continuously monitored at intervals of 10 s, with the powder exposed to the ambient atmosphere (relative humidity of ~30%). The chemically activated HKUST-1 (MC-HK) was also examined using the same procedure.

2.2 Instrumentation

DDW was obtained from a water purification system (Merck Millipore, MQ Direct 8). Diffuse reflectance UV-vis spectra of samples were recorded using an Agilent Cary 5000 UV-VIS-NIR spectrophotometer. PXRD patterns were obtained using a PANalytical

diffractometer (Empyrean) with a monochromatic nickel-filtered Cu K α beam. ^1H -NMR spectra were recorded using an AVANCE III HD FT-NMR spectrometer (Bruker, 400 MHz for ^1H). The ^1H chemical shifts were referenced to the residual proton resonance of the solvent. Nitrogen adsorption/desorption isotherms of the samples were obtained at 77 K by using a Tristar 3020 surface area and porosity analyzer (Micromeritics). The increase in the weight caused by moisture sorption was measured using a microbalance (Sartorius, Cubis Micro Complete Balance). Optical microscope images were taken using an S43T microscope (Bimeince). Raman spectra were recorded using a Nicolet Almega XR dispersive Raman spectrometer (Thermo Scientific). Excitation of the samples was performed by focusing a 1.23-mW 532-nm-wavelength laser beam on a crystal with a 10 \times magnifying objective lens. The instruments used for the PXRD, ^1H -NMR, and Raman analyses are located at the Center for Core Research Facilities (CCRF) in DGIST.

III. RESULTS AND DISCUSSION

1.1 Optical Color Change between Pristine HKUST-1 and Treated HKUST-1

Our first step to address the question was to observe the color change of HKUST-1 after MC treatment without applying heat, assuming that the color change would be significantly influenced by coordination around the Cu^{2+} centers. We observed that whereas pristine HKUST-1 is sky blue, its color turned to deep navy blue after MC treatment (see the optical microscope image and ultraviolet–visible (UV–vis) absorption spectra shown in **Figure 4**). Also notable is that the pattern of the color change after the MC treatment was exactly the same as the pattern after TA which has been a unique method to completely remove all of the ligated solvents (see **Figure 4**).

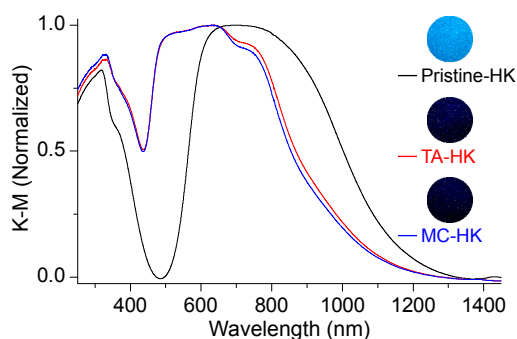


Figure 4. Diffuse reflectance UV-vis absorption spectra of pristine-HK (black curve), TA-HK (red curve), and MC-HK (blue curve) crystalline powders. The circular insets show optical microscope images of the samples as indicated.

The UV-vis absorption of pristine HKUST-1 originates from ligand-to-metal charge transfer (LMCT) and d-d transitions around the Cu^{2+} centers.⁵⁸ The absorption band at energies greater than 2.5 eV (less than approximately 500 nm in wavelength) is due to the LMCT from oxygen in the carboxylate to Cu^{2+} ions, and the absorption band at energies less than 2.5 eV (greater than approximately 500 nm in wavelength) is due to the d-d transition around the Cu^{2+} centers.⁵⁸ The aforementioned color changes are due to the shift of the d-d transition, which, in principle, reflects the changes in the chemical environment around the Cu^{2+} centers (ligand coordination or coordination-free state). More precisely, we speculate that the blue shift is a result of a partial decrease in the number of electrons surrounding Cu^{2+} ion and a loss of degeneracy in d-orbital level arisen by changes in the number of ligand and the geometry around Cu^{2+} center after loss of H_2O and EtOH coordination.⁵⁸⁻⁵⁹ Given that both the TA and MC treatments led to the same extent of blue shift in their absorption spectra, we tentatively speculate that MC itself can function as a reagent for chemical activation of Cu^{2+} centers, thereby forming an intermediate state of MC coordination (more information about this intermediate state is provided in the discussion of our Raman study presented below).

1.2 Structural Stability and Molecules Dissociation of Thermally Treated HKUST-1

¹H-NMR and PXRD tests of a thermally activated HKUST-1 sample were conducted for comparison with the chemical activation results. The NMR data for TA-HK demonstrate that ethanol molecules coordinated to the copper centers in pristine HKUST-1 were removed by

the TA (see **Figure 5a**). The PXRD data indicate that although the coordination bonds were dissociated, the framework of HKUST-1 remained intact (see **Figure 5b**).

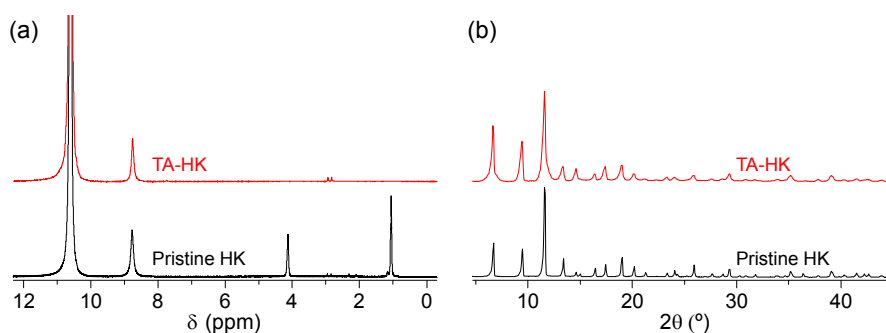


Figure 5. (a) ¹H-NMR spectra and (b) PXRD patterns of pristine-HK and TA-HK powder samples. The TA was performed at 150 °C for 12 h. The NMR spectra were taken after completely dissolving the powder samples in D₂SO₄.

1.3 Structural stability and Surface Areas of Treated HKUST-1

The phase purities of pristine-HK, EtOH-HK, MeOH-HK, and MeCN-HK before and after MC treatment were determined via powder X-ray diffraction (PXRD) measurements (see **Figure 6**). The PXRD patterns of MC-treated samples indicated that the structural integrity of the MOF was well preserved even though the solvent coordination was removed.

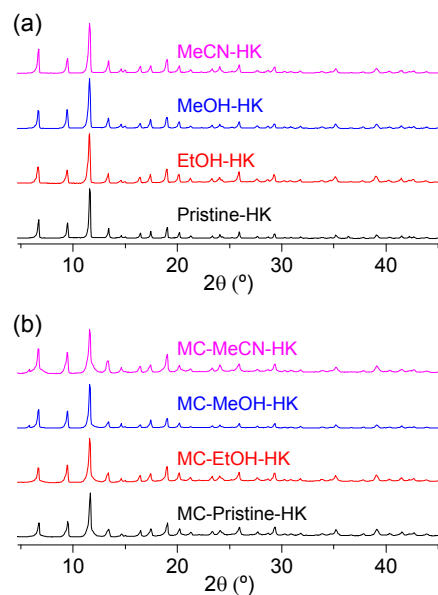


Figure 6. PXRD patterns of pristine-, EtOH-, MeOH-, and MeCN-coordinated HKUST-1 (a) before and (b) after MC treatment.

To confirm this structural integrity, we also tested N₂ isotherms (BET) of both pristine-HK and MC-pristine-HK. Whereas the pristine-HK was treated by TA at 150 °C under vacuum before the BET measurement, the MC-pristine-HK sample was pretreated only by applying vacuum at room temperature. The resulting internal surface area of the samples (approximately 1740 m²·g⁻¹ for TA-Pristine-HK and approximately 1690 m²·g⁻¹ for MC-Pristine-HK) were consistent within the (acceptable) error range (see **Figure 7** and **below** for details). Thus, these PXRD and BET results provide compelling evidence for the safety of MC treatment in terms of structural integrity.

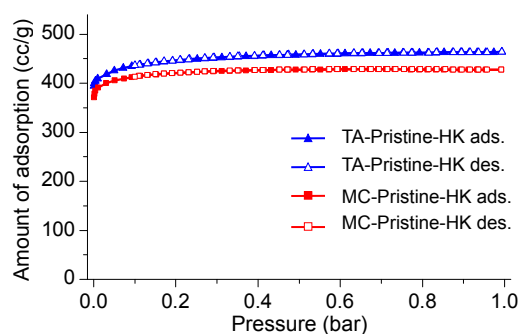


Figure 7. N₂ adsorption/desorption isotherms of TA-HK and MC-HK powders, as indicated.

We wanted to examine whether chemical activation by MC can be achieved at room temperature and whether the framework of the MOF is well preserved after the chemical activation. For this purpose, we tested the N₂ adsorption/desorption isotherm of an MC-pristine-HK powder after evacuating the powder under vacuum at 25 °C for only 2 h. A TA-pristine-HK powder after evacuating the powder under vacuum at 25 °C for only 2 h. A TA-pristine-HK sample was also examined for comparison. The TA-pristine-HK sample was prepared by evacuating it under vacuum at a temperature of 150 °C for 12 h. With the isotherm results in hand, we determined Brunauer–Emmet–Teller (BET) specific surface areas of both MC-pristine-HK and TA-pristine-HK. Specifically, the BET areas were successfully obtained from the linear range of $0.0013 < P/P_0 < 0.0507$ for TA-pristine-HK and $0.0012 < P/P_0 < 0.0313$ for MC-pristine-HK, which pressure ranges were already identified by established “consistency criteria”.⁶⁰⁻⁶² Eventually, we found that both samples yielded similar BET results, i.e., specific surface areas of approximately $1740 \text{ m}^2 \cdot \text{g}^{-1}$ for TA-pristine-HK and approximately $1690 \text{ m}^2 \cdot \text{g}^{-1}$ for MC-pristine-HK. These values are consistent within the (acceptable) error (see **Figure 7**). Additionally, the experimental values were in good agreement with values reported in the literature.⁶³⁻⁶⁶ This result indicates that MC

treatment is a great method to activate the OCSs in HKUST-1 without structural damage.

1.4 $^1\text{H-NMR}$, Raman, and BET Results for Room Temperature Evacuation of HKUST-1

To examine whether the open-metal site of Cu^{2+} ion can be activated at room temperature without MC treatment, we checked $^1\text{H-NMR}$, Raman, and BET of a pristine HKUST-1 sample after applying only vacuum to the sample at room temperature for 2 h (without MC treatment). The $^1\text{H-NMR}$ and Raman spectra of the sample support that EtOH molecules bound to Cu^{2+} centers still remain as coordinated (see **Figure 8**). BET result also demonstrates that applying only vacuum is not a good choice for activating HKUST-1 sample, showing its extremely low internal surface area (approximately $55 \text{ m}^2\cdot\text{g}^{-1}$; compare this value with $1740 \text{ m}^2\cdot\text{g}^{-1}$ for TA-pristine-HK and $1690 \text{ m}^2\cdot\text{g}^{-1}$ for MC-pristine-HK described in **Section 1.3**). Also we note that, the acquisition time of measuring BET for the sample was too long to continue on the measurement (the acquisition time exceeded 90 hours, and the 90 h was a limit for the acquisition of the BET equipment that we used).

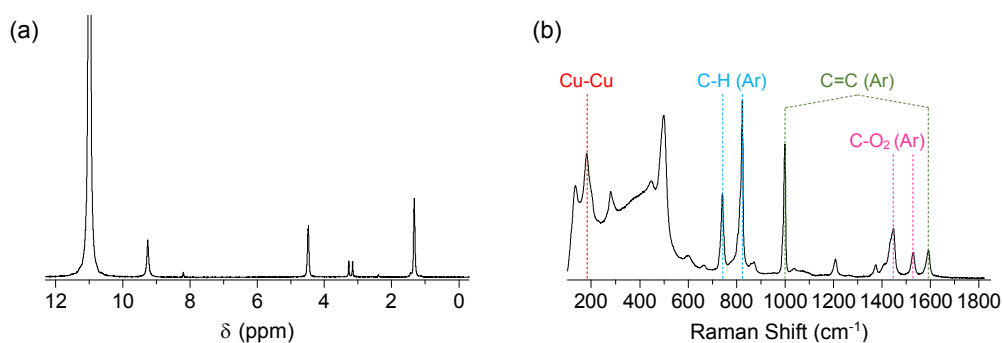


Figure 8. (a) ^1H -NMR and (b) Raman spectra of pristine-HK sample after applying only vacuum at room temperature for 2 h. The NMR spectrum was taken after completely dissolving the powder samples in D_2SO_4 .

1.5 The Surest Evidence of Molecules Dissociation for MC treated HKUST-1

To provide concrete evidence for the chemical activation behavior of MC, we employed ^1H -nuclear magnetic resonance (NMR) spectroscopic analysis. For systematic analyses, we prepared pure EtOH-, MeOH-, and MeCN-coordinated HKUST-1 (EtOH-HK, MeOH-HK, and MeCN-HK, respectively; HK = fully desolvated HKUST-1) and MC-treated EtOH-HK, MeOH-HK, and MeCN-HK (MC-EtOH-HK, MC-MeOH-HK, and MC-MeCN-HK, respectively). Thermally activated HKUST-1 (TA-HK) was also prepared for comparison. Both the H_2O and EtOH in pristine-HK were preferentially removed via TA at $150\text{ }^\circ\text{C}$ for 12 h under vacuum. The TA-HK samples were then placed in a moisture-free Ar-charged glovebox and allowed to coordinate with pure EtOH, MeOH, or MeCN by soaking in the corresponding neat solvent to prepare EtOH-HK, MeOH-HK, and MeCN-HK (see **Figure 2** for details). MC treatment of pristine-HK, EtOH-HK, MeOH-HK, and MeCN-HK was performed by soaking the corresponding powder sample in pure MC solvent at room

temperature for 5 min, and this procedure was repeated 5 times to ensure the completeness of the treatment. **Figure 9** shows $^1\text{H-NMR}$ spectra of pristine-HK, EtOH-HK, MeOH-HK, MeCN-HK, MC-pristine-HK, MC-EtOH-HK, MC-MeOH-HK, and MC-MeCN-HK. The spectra were taken after each powder sample was dissolved in deuterated sulfuric acid, D_2SO_4 .²³ Whereas the peak for the three identical protons in BTC appears at 8.8 ppm, peaks for the two identical CH_2 protons and three identical CH_3 protons in EtOH appear at 4.1 and 1.1 ppm, respectively. In addition, the peaks for the three identical CH_3 protons in MeOH and MeCN appear at 3.7 and 2.1 ppm, respectively. The peak for the protons in water and the hydroxyl group in alcohols appears at ~ 10.6 ppm because the proton forms hydronium ion (H_3O^+) by combining with sulfuric acid. As expected, the peaks for EtOH in pristine-HK disappeared after TA was performed (see the $^1\text{H-NMR}$ spectrum presented in **Section 1.2**). It is also interesting that the spectrum of MC-pristine-HK is identical to the spectrum of TA-HK. We observed that this behavior was generic for all of the MC-EtOH- HK, MC-MeOH-HK, and MC-MeCN-HK samples (see **Figure 9b**). These results thus underscore the ability of MC to perform chemical activation of OCSs.

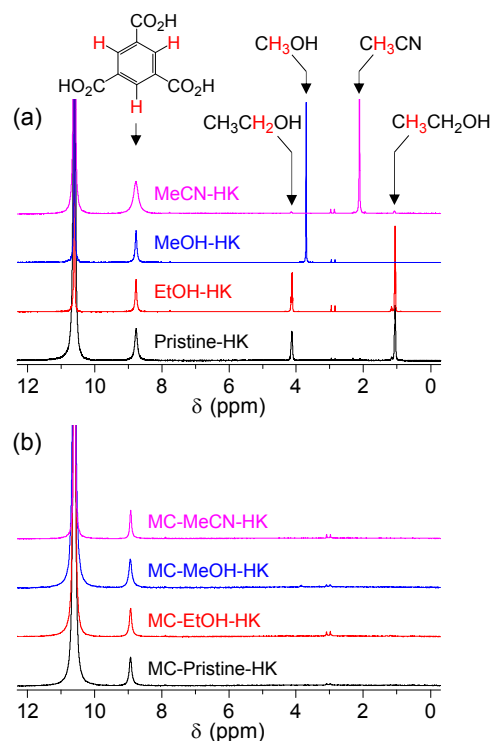


Figure 9. $^1\text{H-NMR}$ spectra of pristine-, EtOH-, MeOH-, and MeCN-coordinated HKUST-1 (a) before and (b) after MC treatment. The NMR spectra were taken after completely dissolving the powder samples in D_2SO_4 .

1.6 Raman Spectra and Water sorption Experiments of HKUST-1

We hypothesized that the change in coordination around the Cu^{2+} centers (presence or absence of the extracoordination of solvents) would be reflected in the vibrational strength of the Cu–Cu bonding. To test this hypothesis, we monitored Raman spectra of pristine-HK before and after MC treatment. A TA-pristine- HK sample was also examined for comparison. To avoid exposure to a moist atmosphere, we prepared the Raman samples by sealing them in disc-shaped quartz containers under the moisture-free conditions of an Ar-charged glovebox. Whereas the stretching vibration mode of Cu–Cu bonding in the pristine-HK appeared at the

shift of approximately 178 cm^{-1} , the stretching vibrations in both MC-pristine-HK and TA-pristine-HK samples appeared at similar shifts of approximately 233 cm^{-1} (see **Figure 12a** and **12b**).⁵⁸ We note that the peak that appeared at 289 cm^{-1} was due to the scissoring vibration mode of Cl–C–Cl in MC (See **Figure 10**). The experimental values of 178 and 233 cm^{-1} agree well with the values theoretically calculated for the vibration mode of H_2O coordinated (211 cm^{-1}) and open-state (233 cm^{-1}) Cu–Cu centers, respectively (see **Figure 13**). This seemingly similar trend is highly consistent with the trend in the above NMR results. Nevertheless, it was interesting that in terms of the Raman shift, a pristine-HK sample wet in pure MC solvent was strikingly different from a dry version of the sample. The Raman shift of MC-wet HKUST-1 appeared at approximately 219 cm^{-1} (see **Figure 12a** and **12b**), thus demonstrating the presence of MC-coordination as an intermediate state. This observation reasonably supports our primary postulate: coordination and decooordination of MC during the MC treatment process. That is, a sequential two-step reaction — coordination of MC through the Cl-bridge formed after replacement of the pre-coordinated solvents and subsequent spontaneous decooordination of MC — is a plausible mechanism for the chemical activation process (see **Section 1.8**).^{50–54} Using Badger’s rule, we could also estimate that the bond strength of the Cu–Cu bonding decreases in the following order: activated-HK > MC-coordinated-HK > pristine-HK.

In addition, we wondered whether the Raman vibrational mode at approximately 289 cm^{-1} in the sample of MC-HK (in MC) is a characteristic of the Cu-Cu paddle-wheel or MC. To determine the origin of the mode, we performed Raman analysis with bare MC solvent. The

Raman spectrum in **Figure 10** shows that the shift at approximately 289 cm^{-1} is the characteristic of the scissoring vibration of Cl-C-Cl.⁶⁷ The spectrum also shows a stretching vibration mode at approximately 705 cm^{-1} , twist vibration mode of H-C-H at approximately 1150 cm^{-1} , and scissoring vibration mode of H-C-H at approximately 1415 cm^{-1} .⁶⁷

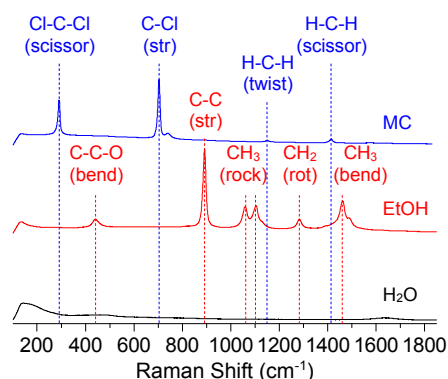


Figure 10. Raman spectra of MC, ethanol (EtOH), and water (H₂O), as indicated.

Another clue regarding the chemical activation is the presence/absence of the open-state of the OCSs that are formed after MC treatment. The presence of the open-state can be checked by monitoring the coordination of moist H₂O molecules in an activated sample. We examined the weight increase of the MC-treated HKUST-1 sample after exposing to moist air (relative humidity = ca. 30%). The test showed an instantaneous increase in weight by ~42% (see **Figure 11c**). Here, we noted an inflection point appearing at ~8.7% because this value is very close to the value (8.9%) theoretically calculated for the maximum amount of H₂O coordinating at the OCSs. (We assumed that weight increase by the coordination of O₂, N₂, CO, CO₂, and other gases in ambient air is likely to be negligible.) Thus, the inflection point indicates that most OCSs in the MC-treated sample remains in the open-state

after the chemical activation. We attribute the further increase over 8.7% to the pore filling of moist water. A similar pattern of weight increase was observed for the TA-HK sample (see **Figure 11c**). Furthermore, coordination of moist H₂O was directly observed via Raman spectroscopy. Whereas the initial peak at 233 cm⁻¹ (open-state) gradually decreased, the peak at 178 cm⁻¹ (H₂O-coordinated) gradually increased as the exposure time to ambient air increased (see **Figure 11d** and **Figure 12**). Also notable is that the peaks were ratiometric at independent positions rather than continuously shifting from 233 to 178 cm⁻¹. This thereby demonstrates that although all Cu²⁺ centers in HKUST-1 are interconnected through BTC ligands, the Cu–Cu vibrations are not interactive.

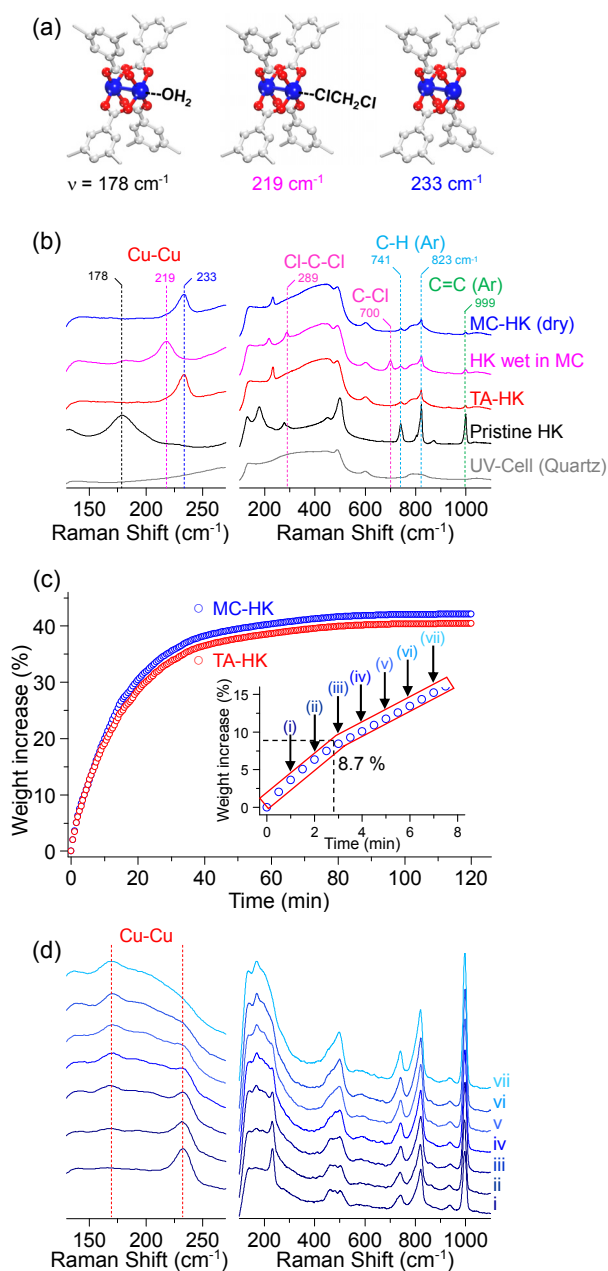


Figure 11. (a) Illustration of H₂O-coordinated, CH₂Cl₂-coordinated, and ligand-free (Cu^{II})₂ centers. (b) Expanded (left panel) and wide (right panel) views of Raman spectra obtained from bare quartz container (gray curve), pristine-HK (black curve), TA-HK (red curve), HK wet in MC (pink curve), and dry MC-HK (blue curve) samples. (c) Plots of increase in the weights of the TA-HK and MC-HK samples with respect to the exposure time to ambient atmosphere (approximately 30% relative humidity). The inset shows the weight change of the MC-HK sample in the initial exposure. (d) Expanded (left panel) and wide (right panel) views of the spectral changes in the Raman shifts of a

dry MC-HK sample according to the exposure time to ambient atmosphere in intervals of 3 min [i.e., after (i) 0, (ii) 3, (iii) 6, (iv) 9, (v) 12, (vi) 15, and (vii) 18 min].

1.7 Raman Spectra of Activated HKUST-1 after Exposure to Ambient Atmosphere

Figure 11d indicates that exposure of MC-HK to ambient atmosphere made the ligand-free Cu^{II} centers effectively re-coordinate with moist water molecules. At this point, we wondered whether the Raman shift of the stretching Cu-Cu vibration mode could eventually be recovered from a higher frequency (233 cm^{-1}) to a lower frequency (178 cm^{-1}) after longer exposure time to the ambient atmosphere. Obviously, we observed that the Raman peak shifted back to the lower frequency. We also found that a thermally activated HKUST-1 (TA-HK) sample exhibited the same behavior. Based on these results, we conclude that the Raman shift of the Cu-Cu vibration is reversible, depending upon the coordination fashion.

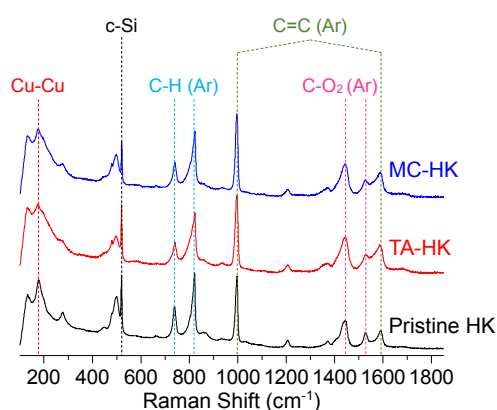


Figure 12. Raman spectra of pristine-HK, TA-HK, and MC-HK powder samples taken after exposure to ambient atmosphere for 2 h. We employed a crystalline silicon substrate for the powder sample in order to utilize the substrate as an internal standard.

1.8 Theoretical Studies for Raman Shift of Cu-Cu vibration in HKUST-1

To gain better understanding of the experimental results (see **Figures 12a** and **12b**), we tried to simulate bond lengths and vibrational frequencies [$d_{\text{Cu-Cu}(X)}$ and $\nu_{\text{Cu-Cu}(X)}$, respectively; X = H₂O, MC (CH₂Cl₂), or OS (open-state: absence of coordinated molecule)] of H₂O-coordinated, MC-coordinated and open-state Cu-Cu in HKUST-1. The simulation was performed using density functional theory (DFT) with projector augmented wave (PAW) pseudopotentials,⁶⁸⁻⁶⁹ as implemented in the Vienna *ab initio* simulation package (VASP) code.⁷⁰ To incorporate an effect of exchange-correlation into the simulation, we employed the generalized gradient approximation (GGA) of PBE.⁷¹ To simplify the simulation, we confined the space of a unit cell (for periodic model calculation) or a cluster (for cluster model calculation) only to a single k-point (the gamma point). Stretching vibrational frequencies of Cu-Cu bond were determined by calculating harmonic oscillation on the basis of the cluster-formation energy curves (see **Figure 13**).⁷² Initially, we calculated bond length of open-state Cu-Cu bonding, $d_{\text{Cu-Cu}(OS)}$, on the basis of periodic model in which whole 624 atoms within a unit cell of HKUST-1 are treated. The resulting $d_{\text{Cu-Cu}(OS)}$ was 2.492 Å. We, however, could not succeed in obtaining stretching vibrational frequency of the Cu-Cu bond, $\nu_{\text{Cu-Cu}(OS)}$, with this periodic model because the number of the atoms in the unit cell was too large to be treated in the simulation process. Instead, we simulated it on the basis of an alternative model: cluster model in which the objective is finitely limited to a cluster consisting of a Cu-Cu paddle-wheel node and four BTC ligands (see inset of **Figure 13** below). This cluster contains only 74 atoms—2 coppers, 24 oxygens, 36 carbons, and 12

hydrogens. This model could enable us to reduce time cost for the calculation and thereby, obtain reliable results. For instance, this model engendered $\nu_{\text{Cu-Cu-(OS)}}$ of 233 cm^{-1} . This value was quite close (or same) to the value (233 cm^{-1}) obtained from our Raman experiments (see **Figure 12** and **Table I**). Thus, we tentatively concluded that the cluster model can be suitably allowed for these simulations. In addition, this model resulted in a theoretical $d_{\text{Cu-Cu-(OS)}}$ value of 2.456 \AA . We wonder how the coordination of water molecule affects the bond length and vibrational frequency of Cu-Cu bond. With this question in mind, we firstly tested a simulation after placing two water molecules around axial open coordination sites (OCSs) of the paired Cu^{2+} centers in the modelled cluster. Consequently, the average $d_{\text{Cu-Cu-(H}_2\text{O)}}$ was calculated to be 2.528 \AA (see **Table I**). This value indicates that the bond length is slightly elongated after water coordination (compare this 2.528 \AA with the aforementioned $d_{\text{Cu-Cu-(OS)}}$ value of 2.456 \AA). Regardless, a subsequently calculated bond length (2.216 \AA) between Cu^{2+} and oxygen atom in H_2O molecule agreed with an experimental value (2.165 \AA) previously reported in the literature.²⁷ This implies that this calculation method is highly reliable, and thus the simulated $d_{\text{Cu-Cu-(H}_2\text{O)}}$ value itself and the elongation behavior after water coordination are acceptable. A further calculation for $\nu_{\text{Cu-Cu-(H}_2\text{O)}}$ resulted in a frequency of 211 cm^{-1} . This value was somewhat higher related to the value obtained from our experiments (178 cm^{-1}). We ascribe this error to complicated vibration modes of the coordinated H_2O molecules. However, the red-shift from higher to lower frequencies after water coordination is an indisputable fact because the shift was commonly observed in both theory and experiment. (Remind the shifts from 233 to 211 cm^{-1} in theoretical calculation and from 233 to 178 cm^{-1}

in experimental observation). We also tried to calculate vibration frequency of MC-coordinated Cu-Cu bond ($\nu_{\text{Cu-Cu-(MC)}}$), but could not obtain successful result due to the complexity of binding modes and vibrations of the coordinated MC molecule in calculations. Nevertheless, given that the aforementioned elongation of Cu-Cu bond and the red-shift of vibration frequency are highly dependent upon coordinating solvents and their coordination modes, we tentatively speculate that the vibrational frequency increases as the coordination strength of Lewis base (LB) molecules decreases. (We note that water molecule is a LB molecule that possesses lone-paired electrons in its oxygen.) We need more systematic studies for this speculation. However, on the basis of the speculation and our experimental results, we also postulate that the coordination strength of MC ($\nu_{\text{Cu-Cu-(MC)}} = 219 \text{ cm}^{-1}$) is weaker than that of H₂O ($\nu_{\text{Cu-Cu-(H}_2\text{O)}} = 178 \text{ cm}^{-1}$), and thereby MC can be readily de-coordinated from the Cu²⁺ center with a low activation energy (thermal energy at room temperature).

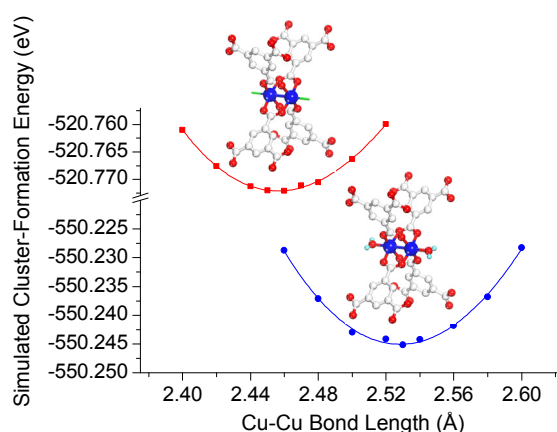

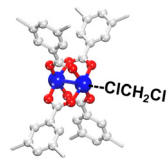
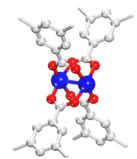


Figure 13. Raman spectra of MC, ethanol (EtOH), and water (H₂O), as indicated.

Table I. Bond Length ($d_{\text{Cu-Cu}}$) and Stretching Vibration Frequency ($\nu_{\text{Cu-Cu}}$) of Cu-Cu Bonding in HKUST-1.

Physical parameters	Theory/Experiment	Coordination mode		
		H ₂ O-HKUST-1	MC-HKUST-1	Open-HKUST-1
				
Bond length	Periodic model	-	-	2.492
$d_{\text{Cu-Cu}}$ (Å)	Cluster model	2.528	-	2.456
	Experiments	2.628 ²⁷	-	
Vibration frequencies	Cluster model	211	-	233
$\nu_{\text{Cu-Cu}}$ (cm ⁻¹)	Experiments	178	219	233

1.9 ¹H-NMR, Raman and BET Result for Room Temperature Evacuation of HKUST-1

To examine whether the open-metal site of Cu²⁺ ion can be activated at room temperature without MC treatment, we checked ¹H-NMR, Raman, and BET of a pristine HKUST-1 sample after applying only vacuum to the sample at room temperature for 2 h (without MC treatment). The ¹H-NMR and Raman spectra of the sample support that EtOH molecules bound to Cu²⁺ centers still remain as coordinated. BET result also demonstrates that applying only vacuum is not a good choice for activating HKUST-1 sample, showing its extremely low internal surface area (approximately 55 m²·g⁻¹; compare this value with 1740 m²·g⁻¹ for TA-pristine-HK and 1690 m²·g⁻¹ for MC-pristine-HK described in **Figure 7**). Also we note that, the acquisition time of measuring BET for the sample was too long to continue on the measurement (the acquisition time exceeded 90 hours, and the 90 h was a limit for the acquisition of the BET equipment that we used).

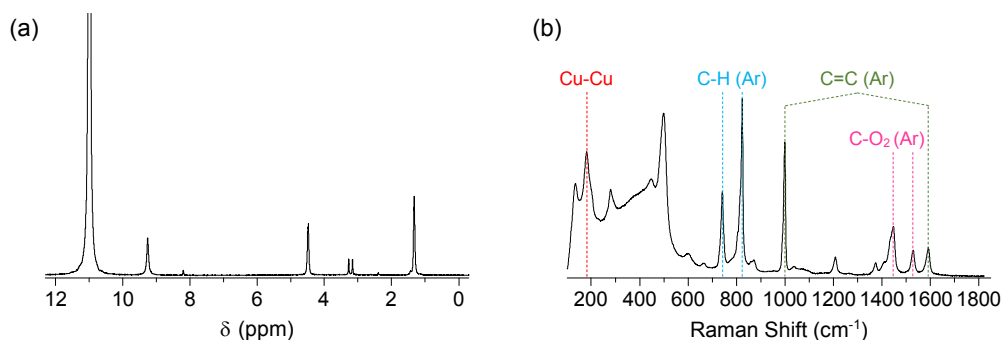


Figure 14. (a) $^1\text{H-NMR}$ and (b) Raman spectra of pristine-HK sample after applying only vacuum at room temperature for 2 h. The NMR spectrum was taken after completely dissolving the powder samples in D_2SO_4 .

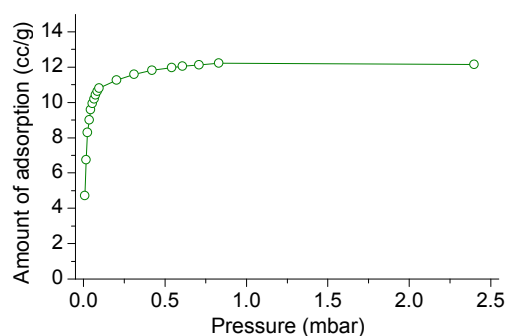


Figure 15. N_2 adsorption isotherms of a pristine-HK sample after applying only vacuum at room temperature for 2 h. We could not obtain a complete data set from BET due to the acquisition time limit of the equipment.

1.10 Application to Cu-MOF-2 with Chemical Activation

We also tested Cu-MOF-2 to address whether the chemical activation behavior of MC could be expanded. Crystalline Cu-MOF-2 powder was synthesized from the sources of $\text{Cu}(\text{NO}_3)_2$ and BDC using DMF solvent. We observed that the color of Cu-MOF-2 changed from light green to dark blue after the sample was thermally activated. The MC treatment also exhibited a similar color change, thus implying its activation function even in Cu-MOF-2

(see **Figure 16a**). UV–vis absorption spectra of the MOF-2 samples clearly indicate that the color change is caused by the blue-shift of the d–d transition, similar to the pattern observed in HKUST-1.⁵⁸ To further understand this behavior, we examined ¹H NMR analysis. The ¹H NMR spectrum of pristine MOF-2 powder shows that it contains DMF as a coordinating component at the OCSs (see **Figure 16b**). Consistent with the above result, the coordinated DMF was dissociated after MC treatment. Meanwhile, the phase of MOF-2 was transformed after the TA process, as previously reported in literature (see **Section 1.11**).⁷³⁻⁷⁴ The chemical activation also resulted in PXRD patterns quite similar to those of the TA, indicating that its 2-dimensional framework was not collapsed after the chemical activation. In terms of the Raman spectra, MOF-2 exhibited behavior that differed from that of HKUST-1 in two aspects (see **Figure 16c**). One aspect is that the Raman shift involving the Cu–Cu stretching vibration appeared as a doublet mode at 196 and 218 cm⁻¹. The other aspect is that whereas HKUST-1 exhibited a blue-shift in the Cu–Cu vibration after activation (from 178 to 233 cm⁻¹), MOF-2 exhibited red-shifts in both peaks of the doublet (from 196 to 191 cm⁻¹ and from 218 to 204 cm⁻¹). Although more comprehensive studies are required to fully understand this behavior, our observation is in good agreement with the pattern reported in the literature.⁷⁴ Regardless, an important fact is that the pattern of the shift after chemical activation is exactly same as the pattern of the shift after TA. This evidence strongly supports our demonstration of the chemical activation behavior of MC in Cu-MOF-2.

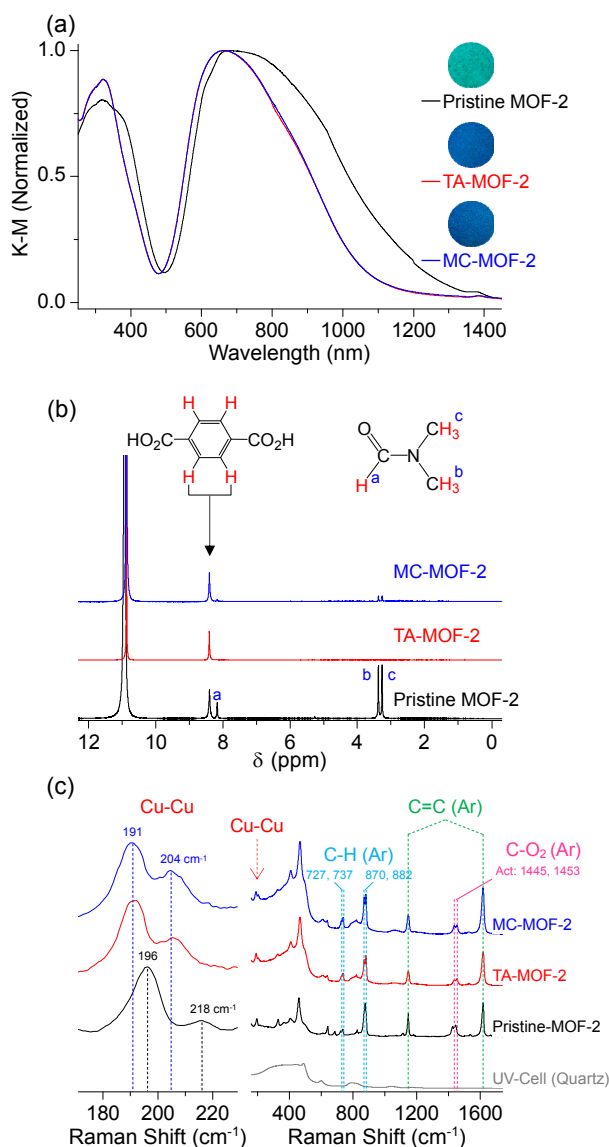


Figure 16. (a) Diffuse reflectance UV-vis absorption spectra of pristine-MOF-2 (black curve), TA-MOF-2 (red curve), and MC-MOF-2 (blue curve) crystalline powders. The optical microscope images in the circular insets display the colors of the powder samples. (b) $^1\text{H-NMR}$ spectra of pristine-MOF-2, TA-MOF-2, and MC-MOF-2 taken after the samples were dissolved in D_2SO_4 . (c) Expanded (left panel) and wide (right panel) views of the Raman spectra of pristine-, TA-, and MC-MOF-2 powder samples. The Raman spectra were taken after the samples were sealed in a moisture-free argon-charged glove box.

1.11 Structural Stability of Treated Cu-MOF-2

To check whether the chemical activation of Cu-MOF-2 engenders behavior similar to TA, we monitored the changes in the PXRD patterns of pristine-, TA-, and MC-MOF-2. The PXRD patterns indicated that although the crystalline phase of the MOF-2 changed after activation, the superficial result of the chemical activation was the same as that of the TA (see **Figure 17**). Although more comprehensive studies are required to fully understand the phase transition behavior, this feature has often been observed.^{57-58,73-74}

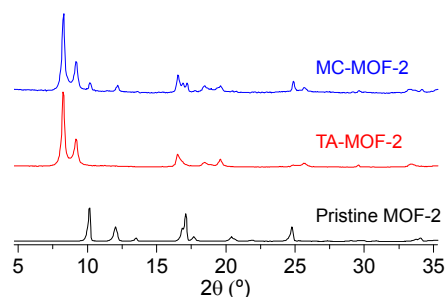


Figure 17. PXRD patterns of pristine-MOF-2, TA-MOF-2, and MC-MOF-2 powder samples, as indicated.

1.12 Application to Large size MOF Films with Chemical Activation

TA, which is typically conducted by applying heat and vacuum, requires effective facilities to make the temperature of the surroundings higher and the pressure lower, at least relative to the atmospheric conditions. In contrast with TA, chemical activation is likely to be more useful when the amount of the powder sample or the size of the MOF films is large because such facilities are not required for this method. To test the feasibility of the MC

treatment, we synthesized HKUST-1 film on metallic Cu substrate via an oxidation reaction (see **Figure 18a, 18b, and 18c**).⁷⁵ Whereas the color of the as-synthesized HKUST-1 film was sky blue, its color changed to dark blue after the MC treatment (see **Figure 18d**). In agreement with the results obtained from powder samples, the chemical activation process could completely remove the coordinated EtOH from the film (**Figure 18e and 18f**) and simultaneously preserve its framework well (**Figure 18g and 18h**).

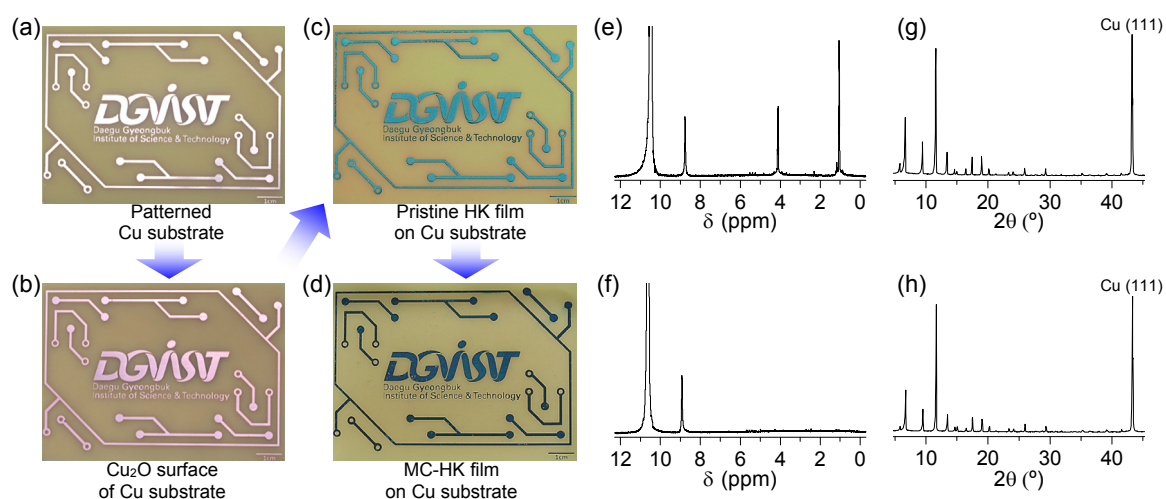


Figure 18. Photographs of the (a) patterned Cu substrate, (b) surface-oxidized Cu substrate (Cu₂O/Cu), (c) pristine HKUST-1 film synthesized on the Cu substrate, and (d) MC-treated HKUST-1 film. ¹H-NMR spectra of (e) pristine- and (f) MC-treated HKUST-1 films. XRD patterns of (e) pristine- and (f) MC-treated HKUST-1 films.

IV. CONCLUSION

In summary, we have observed a “chemical activation” function of MC to remove the solvent coordination from OCSs of metal nodes. For the examples examined, the function of MC was clearly demonstrated not only by monitoring the dissolution of the $^1\text{H-NMR}$ peaks for the solvent molecules coordinated at the OCSs but also by observing the Raman shift of the Cu–Cu vibration. In particular, the Raman studies enabled us to observe the presence of MC coordination as a conceivable intermediate state during the chemical activation reaction. We also confirmed that this chemical activation behavior does not appear if MC treatment is omitted in the process (for instance, when only vacuum is applied at room temperature for 2 h; see **Figure 14** and **Figure 15**). Using HKUST-1 films synthesized on patterned copper plates, we have also demonstrated that this chemical method will be more useful for activating large-area MOF films as a cheap and facile process. We anticipate that this secondary role of MC will also be useful for the MOF industry, and the resulting guidelines will prove transferrable/adaptable to other MOFs that contains ligand-accessible metal ions, such as Zn-HKUST-1, MIL-101 and MOF-74.

V. REFERENCE

1. Yaghi, O. M.; Li, H.; Davis, C.; Richardson, D.; Groy, T. L. “Synthetic Strategies, Structure Patterns, and Emerging Properties in the Chemistry of Modular Porous Solids”, *Acc. Chem. Res.* 1998, **31**, 474–484.
2. O’Keeffe, M.; Yaghi, O. M. “Deconstructing the Crystal Structures of Metal–Organic Frameworks and Related Materials into Their Underlying Nets”, *Chem. Rev.* 2012, **112**, 675–702.
3. Zhou, H.-C.; Long, J. R.; Yaghi, O. M. “Introduction to Metal–Organic Frameworks”, *Chem. Rev.* 2012, **112**, 673–674.
4. Li, M.; Li, D.; O’Keeffe, M.; Yaghi, O. M. “Topological Analysis of Metal–Organic Frameworks with Polytopic Linkers and/or Multiple Building Units and the Minimal Transitivity Principle”, *Chem. Rev.* 2014, **114**, 1343–1370.
5. Deria, P.; Mondloch, J. E.; Karagiari, O.; Bury, W.; Hupp, J. T.; Farha, O. K. “Beyond post-synthesis modification: evolution of metal–organic frameworks via building block replacement”, *Chem. Soc. Rev.* 2014, **43**, 5896–5912.
6. Zhou, H.-C.; Kitagawa, S. “Metal–Organic Frameworks (MOFs)”, *Chem. Soc. Rev.* **2014**, **43**, 5415–5418.
7. Gassensmith, J. J.; Kim, J. Y.; Holcroft, J. M.; Farha, O. K.; Stoddart, J. F.; Hupp, J. T.; Jeong, N. C. “A Metal–Organic Framework-Based Material for Electrochemical Sensing of Carbon Dioxide”, *J. Am. Chem. Soc.* 2014, **136**, 8277–8282.

8. Furukawa, H.; Cordova, K. E.; O’Keeffe, M.; Yaghi, O. M. “The Chemistry and Applications of Metal-Organic Frameworks”, *Science* 2013, **341**, 974.
9. Banerjee, D.; Cairns, A. J.; Liu, J.; Motkuri, R. K.; Nune, S. K.; Fernandez, C. A.; Krishna, R.; Strachan, D. M.; Thallapally, P. K. “Potential of Metal–Organic Frameworks for Separation of Xenon and Krypton”, *Acc. Chem. Res.* 2015, **48**, 211–219.
10. Bae, Y.-S.; Lee, C. Y.; Kim, K. C.; Farha, O. K.; Nickias, P.; Hupp, J. T.; Nguyen, S. T.; Snurr, R. Q. “High Propene/Propane Selectivity in Isostructural Metal–Organic Frameworks with High Densities of Open Metal Sites”, *Angew. Chem., Int. Ed.* 2012, **51**, 1857–1860.
11. D’Alessandro, D. M.; Smit, B.; Long, J. R. “Carbon Dioxide Capture: Prospects for New Materials”, *Angew. Chem., Int. Ed.* 2010, **49**, 6058–6082.
12. Bae, Y.-S.; Snurr, R. Q. “Development and Evaluation of Porous Materials for Carbon Dioxide Separation and Capture”, *Angew. Chem., Int. Ed.* 2011, **50**, 11586–11596.
13. Lin, L.-C.; Kim, J.; Kong, X.; Scott, E.; McDonald, T. M.; Long, J. R.; Reimer, J. A.; Smit, B. “Understanding CO₂ Dynamics in Metal–Organic Frameworks with Open Metal Sites”, *Angew. Chem., Int. Ed.* 2013, **52**, 4410–4413.
14. Dinca, M.; Long, J. R. “Hydrogen Storage in Microporous Metal–Organic Frameworks with Exposed Metal Sites”, *Angew. Chem., Int. Ed.* 2008, **47**, 6766–6779.
15. Eddaoudi, M.; Kim, J.; Rosi, N.; Vodak, D.; Wachter, J.; O’Keeffe, M.; Yaghi, O. M. “Systematic Design of Pore Size and Functionality in Isorecticular MOFs and Their Application in Methane Storage”, *Science* 2002, **295**, 469–472.

16. Peng, Y.; Krungleviciute, V.; Eryazici, I.; Hupp, J. T.; Farha, O. K.; Yildirim, T. “Methane Storage in Metal–Organic Frameworks: Current Records, Surprise Findings, and Challenges”, *J. Am. Chem. Soc.* 2013, **135**, 11887–11894.
17. He, Y.; Zhou, W.; Qian, G.; Chen, B. “Methane storage in metal–organic frameworks”, *Chem. Soc. Rev.* 2014, **43**, 5657–5678.
18. Xiang, S.; Zhou, W.; Zhang, Z.; Green, M. A.; Liu, Y.; Chen, B. “Open Metal Sites within Isostructural Metal–Organic Frameworks for Differential Recognition of Acetylene and Extraordinarily High Acetylene Storage Capacity at Room Temperature”, *Angew. Chem., Int. Ed.* 2010, **49**, 4615–4618.
19. Lee, J.; Farha, O. K.; Roberts, J.; Scheidt, K. A.; Nguyen, S. T.; Hupp, J. T. “Metal–organic framework materials as catalysts”, *Chem. Soc. Rev.* 2009, **38**, 1450–1459.
20. Schlichte, K.; Kratzke, T.; Kaskel, S. “Improved synthesis, thermal stability and catalytic properties of the metal-organic framework compound $\text{Cu}_3(\text{BTC})_2$ ”, *Microporous Mesoporous Mater.* 2004, **73**, 81–88.
21. Feng, D.; Gu, Z.-Y.; Li, J.-R.; Jiang, H.-L.; Wei, Z.; Zhou, H.-C. “Zirconium-Metalloporphyrin PCN-222: Mesoporous Metal–Organic Frameworks with Ultrahigh Stability as Biomimetic Catalysts”, *Angew. Chem., Int. Ed.* 2012, **51**, 10307–10310.
22. Kreno, L. E.; Leong, K.; Farha, O. K.; Allendorf, M.; Van Duyne, R. P.; Hupp, J. T. “Metal–Organic Framework Materials as Chemical Sensors”, *Chem. Rev.* 2012, **112**, 1105–1125.
23. Jeong, N. C.; Samanta, B.; Lee, C. Y.; Farha, O. K.; Hupp, J. T. “Coordination-Chemistry

- Control of Proton Conductivity in the Iconic Metal–Organic Framework Material HKUST-1”, *J. Am. Chem. Soc.* 2012, **134**, 51–54.
24. Ramaswamy, P.; Wong, N. E.; Shimizu, G. K. H. “MOFs as proton conductors – challenges and opportunities”, *Chem. Soc. Rev.* 2014, **43**, 5913–5932.
25. Mondloch, J. E.; Bury, W.; Fairen-Jimenez, D.; Kwon, S.; DeMarco, E. J.; Weston, M. H.; Sarjeant, A. A.; Nguyen, S. T.; Stair, P. C.; Snurr, R. Q.; Farha, O. K.; Hupp, J. T. “Vapor-Phase Metalation by Atomic Layer Deposition in a Metal–Organic Framework”, *J. Am. Chem. Soc.* 2013, **135**, 10294–10297.
26. Barea, E.; Montoro, C.; Navarro, J. A. R. “Toxic gas removal – metal–organic frameworks for the capture and degradation of toxic gases and vapours”, *Chem. Soc. Rev.* 2014, **43**, 5419–5430.
27. Chui, S. S.-Y.; Lo, S. M.-F.; Charmant, J. P. H.; Orpen, A. G.; Williams, I. D. “A Chemically Functionalizable Nanoporous Material $[\text{Cu}_3(\text{TMA})_2(\text{H}_2\text{O})_3]_n$ ”, *Science* 1999, **283**, 1148–1150.
28. Eddaoudi, M.; Li, H.; Yaghi, O. M. “Highly Porous and Stable Metal-Organic Frameworks: Structure Design and Sorption Properties”, *J. Am. Chem. Soc.* 2000, **122**, 1391–1397.
29. Yazaydin, A. O.; Benin, A. I.; Faheem, S. A.; Jakubczak, P.; Low, J. J.; Willis, R. R.; Snurr, R. Q. “Enhanced CO_2 Adsorption in Metal-Organic Frameworks via Occupation of Open-Metal Sites by Coordinated Water Molecules”, *Chem. Mater.* 2009, **21**, 1425–1430.

30. Canivet, J.; Fateeva, A.; Guo, Y.; Coasne, B.; Farrusseng, D. “Water adsorption in MOFs: fundamentals and applications”, *Chem. Soc. Rev.* 2014, **43**, 5594–5617.
31. Borfecchia, E.; Maurelli, S.; Gianolio, D.; Groppo, E.; Chiesa, M.; Bonino, F.; Lamberti, C. “Insights into Adsorption of NH₃ on HKUST-1 Metal–Organic Framework: A Multitechnique Approach”, *J. Phys. Chem. C* 2012, **116**, 19839–19850.
32. Xiao, B.; Wheatley, P. S.; Zhao, X.; Fletcher, A. J.; Fox, S.; Rossi, A. G.; Megson, I. L.; Bordiga, S.; Regli, L.; Thomas, K. M.; Morris, R. E. “High-Capacity Hydrogen and Nitric Oxide Adsorption and Storage in a Metal-Organic Framework”, *J. Am. Chem. Soc.* 2007, **129**, 1203–1209.
33. de Lima, G. F.; Mavrandonakis, A.; de Abreu, H. A.; Duarte, H. A.; Heine, T. “Mechanism of Alcohol–Water Separation in Metal–Organic Frameworks”, *J. Phys. Chem. C* 2013, **117**, 4124–4130.
34. Munch, A. S.; Mertens, F. O. R. L. “HKUST-1 as an open metal site gas chromatographic stationary phase—capillary preparation, separation of small hydrocarbons and electron donating compounds, determination of thermodynamic data”, *J. Mater. Chem.* 2012, **22**, 10228–10234.
35. Supronowicz, B.; Mavrandonakis, A.; Heine, T. “Interaction of Small Gases with the Unsaturated Metal Centers of the HKUST-1 Metal Organic Framework”, *J. Phys. Chem. C* 2013, **117**, 14570–14578.
36. Supronowicz, B.; Mavrandonakis, A.; Heine, T. “Interaction of Biologically Important Organic Molecules with the Unsaturated Copper Centers of the HKUST-1

- Metal–Organic Framework: an Ab-Initio Study”, *J. Phys. Chem. C* 2015, **119**, 3024–3032.
37. Yang, Y.; Shukla, P.; Wang, S.; Rudolph, V.; Chen, X.-M.; Zhu, Z. “Significant improvement of surface area and CO₂ adsorption of Cu–BTC *via* solvent exchange activation”, *RSC Adv.* 2013, **3**, 17065–17072.
38. Mondloch, J. E.; Karagiari, O.; Farha, O. K.; Hupp, J. T. “Activation of metal–organic framework materials”, *CrystEngComm* 2013, **15**, 9258–9264.
39. Abrahams, B. F.; Hoskins, B. F.; Michail, D. M.; Robson, R. “Assembly of porphyrin building blocks into network structures with large channels”, *Nature* 1994, **369**, 727–729.
40. Li, H.; Eddaoudi, M.; Groy, T. L.; Yaghi, O. M. “Establishing Microporosity in Open Metal-Organic Frameworks: Gas Sorption Isotherms for Zn(BDC)(BDC=1,4-Benzenedicarboxylate)”, *J. Am. Chem. Soc.* 1998, **120**, 8571–8572.
41. Kepert, C. J.; Rosseinsky, M. J. “Zeolite-like crystal structure of an empty microporous molecular framework”, *Chem. Commun.* 1999, 375–376.
42. Ferey, G.; Mellot-Draznieks, C.; Serre, C.; Millange, F.; Dutour, J.; Surble, S.; Margiolaki, I. “A Chromium Terephthalate–Based Solid with Unusually Large Pore Volumes and Surface Area”, *Science* 2005, **309**, 2040–2042.
43. Cavka, J. H.; Jakobsen, S.; Olsbye, U.; Guillou, N.; Lamberti, C.; Bordiga, S.; Lillerud, K. P. “A New Zirconium Inorganic Building Brick Forming Metal Organic Frameworks with Exceptional Stability”, *J. Am. Chem. Soc.* 2008, **130**, 13850–13851.

44. Li, H.; Eddaoudi, M.; O’Keeffe, M.; Yaghi, O. M. “Design and synthesis of an exceptionally stable and highly porous metal-organic framework”, *Nature* 1999, **402**, 276–279.
45. Nelson, A. P.; Farha, O. K.; Mulfort, K. L.; Hupp, J. T. “Supercritical Processing as a Route to High Internal Surface Areas and Permanent Microporosity in Metal-Organic Framework Materials”, *J. Am. Chem. Soc.* 2009, **131**, 458–460.
46. Lohe, M. R.; Rose, M.; Kaskel, S. “Metal–organic framework (MOF) aerogels with high micro- and macroporosity”, *Chem. Commun.* 2009, 6056–6058.
47. Morris, W.; Voloskiy, B.; Demir, S.; Gandara, F.; McGrier, P.L.; Furukawa, H.; Cascio, D.; Stoddart, J. F.; Yaghi, O. M. “Synthesis, Structure, and Metalation of Two New Highly Porous Zirconium Metal–Organic Frameworks”, *Inorg. Chem.* 2012, **51**, 6443–6445.
48. Tsao, C.-S.; Chen, C.-Y.; Chung, T.-Y.; Su, C.-J.; Su, C.-H.; Chen, H.-L.; Jeng, U.-S.; Yu, M.-S.; Liao, P.-Y.; Lin, K.-F.; Tzeng, Y.-R. “Structural Analysis and Thermal Behavior of Pore Networks in High-Surface-Area Metal-Organic Framework”, *J. Phys. Chem. C* 2010, **114**, 7014–7020.
49. Bhunia, M. K.; Hughes, J. T.; Fetting, J. C.; Navrotsky, A. “Thermochemistry of Paddle Wheel MOFs: Cu-HKUST-1 and Zn-HKUST-1”, *Langmuir* 2013, **29**, 8140–8145.
50. Colman, M. R.; Noirot, M. D.; Miller, M. M.; Anderson, O. P.; Strauss, S. H. “Lewis Basicity of the "Noncoordinating" Common Solvent 1,2-Dichloroethane: Strong RCI

- Ag Bonding in $\text{AgOTeF}_5(1,2\text{-C}_2\text{H}_4\text{Cl}_2)$ ”, *J. Am. Chem. Soc.* 1988, **110**, 6886–6888.
51. Newbound, T. D.; Colsman, M. R.; Miller, M. M.; Wulfsberg, G. P.; Anderson, O. P.; Strauss, S. H. “Dichloromethane Is a Coordinating Solvent”, *J. Am. Chem. Soc.* 1989, **111**, 3762–3764.
52. Honeychuck, R. V.; Hersh, W. H. “Observation of Anion Spinning in the Dynamic ^{31}P NMR Spectra of Fluorine-Bridged SbF_6^- , BF_4^- , and PF_6^- Adducts of $\text{R}_3\text{P}(\text{CO})_3(\text{NO})\text{W}^+$. Implications for Barriers to Ionization and the Formation of Ion Pairs and Free Ions in Methylene Chloride and Hexane Solution”, *J. Am. Chem. Soc.* 1989, **111**, 6056–6070.
53. Colsman, M. R.; Newbound, T. D.; Marshall, L. J.; Noirot, M. D.; Miller, M. M.; Wulfsberg, G. P.; Frye, J. S.; Anderson, O. P.; Strauss, S. H. “Silver(I) Complexes of Dichloromethane and 1,2-Dichloroethane”, *J. Am. Chem. Soc.* 1990, **112**, 2349–2362.
54. Huhmann-Vincent, J.; Scott, B. L.; Kubas, G. J. “Rhenium Complexes with Weakly Coordinating Solvent Ligands, *cis*- $[\text{Re}(\text{PR}_3)(\text{CO})_4(\text{L})][\text{BAR}_\text{F}]$, $\text{L}=\text{CH}_2\text{Cl}_2$, Et_2O , NC_5F_5 : Decomposition to Chloride-Bridged Dimers in CH_2Cl_2 Solution”, *Inorg. Chem.* 1999, **38**, 115–124.
55. Mori, W.; Inoue, F.; Yoshida, K.; Nakayama, H.; Takamizawa, S.; Kishita, M. “Synthesis of New Adsorbent Copper(II) Terephthalate”, *Chem. Lett.* 1997, **27**, 1219–1220.
56. Seki, K.; Takamizawa, S.; Mori, W. “Characterization of Microporous Copper(II) Dicarboxylates (Fumarate, Terephthalate, and *trans*-1,4-Cyclohexanedicarboxylate) by Gas Adsorption”, *Chem. Lett.* 2001, **30**, 122–123.
57. Carson, C. G.; Hardcastle, K.; Schwartz, J.; Liu, X.; Hoffmann, C.; Gerhardt, R. A.;

- Tannenbaum, R. "Synthesis and Structure Characterization of Copper Terephthalate Metal–Organic Frameworks", *Eur. J. Inorg. Chem.* 2009, 2338–2343.
58. Prestipino, C.; Regli, L.; Vitillo, J. G.; Bonino, F.; Damin, A.; Lamberti, C.; Zecchina, A.; Solari, P. L.; Kongshaug, K. O.; Bordiga, S. "Local Structure of Framework Cu(II) in HKUST-1 Metallorganic Framework: Spectroscopic Characterization upon Activation and Interaction with Adsorbates", *Chem. Mater.* 2006, **18**, 1337–1346.
59. Huheey, J. E.; Keiter, E. A.; Keiter, R. L. *Inorganic Chemistry: Principles of Structure and Reactivity*, 4th ed.; HarperCollins College: New York, 1993; p 404.
60. Rouquerol, J.; Llewellyn, P.; Rouquerol, F. "Is the BET equation applicable to microporous adsorbent?", *Stud. Surf. Sci. Catal.* 2007, **160**, 49-56.
61. Walton, K.S.; Snurr, R.Q. "Applicability of the BET Method for Determining Surface Areas of Microporous Metal-Organic Frameworks", *J. Am. Chem. Soc.* 2007, **129**, 8552-8556.
62. Bae, Y.-S.; Yazaydin, A.O.; Snurr, R.Q. "Evaluation of the BET Method for Determining Surface Areas of MOFs and Zeolites that Contain Ultra-Micropores", *Langmuir* 2010, **26**, 5475-5483.
63. Panella, B.; Hirscher, M.; Putter, H.; Muller, U. "Hydrogen Adsorption in Metal–Organic Frameworks: Cu-MOFs and Zn-MOFs Compared", *Adv. Funct. Mater.* 2006, **16**, 520-524.
64. Ma, S.; Zhou, H.-C. "Gas storage in porous metal–organic frameworks for clean energy applications", *Chem. Commun.* 2010, **46**, 44-53.

65. Klimakow, M.; Klobes, P.; Thunemann, A. F.; Rademann, K.; Emmerling, F. “Mechanochemical Synthesis of Metal-Organic Frameworks: A Fast and Facile Approach toward Quantitative Yields and High Specific Surface Areas”, *Chem. Mater.* 2010, **22**, 5216-5221.
66. Song, X.; Jeong, S.; Kim, D.; Lah, M. S. “Transmetalations in two metal–organic frameworks with different framework flexibilities: Kinetics and core–shell heterostructure”, *CrystEngComm.* 2012, **14**, 5753-5756.
67. Shimanouchi, T. *Tables of Molecular Vibrational Frequencies Consolidated Volume I, National Bureau of Standards* **1972**, pp 1-160.
68. Blochl, P. E. “Projector augmented-wave method”, *Phys. Rev. B* 1994, **50**, 17953-17979.
69. Kresse, G.; Joubert, D. “From ultrasoft pseudopotentials to the projector augmented-wave method”, *Phys. Rev. B* 1999, **59**, 1758-1775.
70. Kresse, G.; Furthmuller, J. “Efficient iterative schemes for ab initio total-energy calculations using a plane-wave basis set”, *Phys. Rev. B* 1996, **54**, 11169-11186.
71. Perdew, J. P.; Burke, K.; Ernzerhof, M. “Generalized Gradient Approximation Made Simple”, *Phys. Rev. Lett.* 1996, **77**, 3865-3868.
72. Van de Walle, C. G. “Energetics and Vibrational Frequencies of Interstitial H₂ Molecules in Semiconductors”, *Phys. Rev. Lett.* 1998, **80**, 2177-2180.
73. Chen, Z.; Xiang, S.; Zhao, D.; Chen, B. “Reversible Two-Dimensional-Three Dimensional Framework Transformation within a Prototype Metal-Organic Framework”, *Cryst. Growth Des.* 2009, **9**, 5293–5296.

74. Tan, K.; Nijem, N.; Canepa, P.; Gong, Q.; Li, J.; Thonhauser, T.; Chabal, Y. J. “Stability and Hydrolyzation of Metal Organic Frameworks with paddle-Wheel SBUs upon Hydration”, *Chem. Mater.* 2012, **24**, 3153–3167.
75. Okada, K.; Ricco, R.; Tokudome, Y.; Styles, M. J.; Hill, A. J.; Takahashi, M.; Falcaro, P. “Copper Conversion into Cu(OH)₂ Nanotubes for Positioning Cu₃(BTC)₂ MOF Crystals: Controlling the Growth on Flat Plates, 3D Architectures, and as Patterns”, *Adv. Funct. Mater.* 2014, **24**, 1969–1977.

요 약 문

구리 기반의 금속 유기 구조체 내의 Open Metal Sites의 화학적 경로를 통한 화학적 활성화

금속 유기 구조체는 골격을 이루는 유기 리간드와 이들 리간드 등을 서로 연결하는 금속 이온 또는 금속 산화물 클러스터들이 서로 자가 조립을 통해 3차원적으로 결정 구조화된 나노 다공성 물질을 일컫는다. 금속 유기 구조체는 각 구조체마다 특정 모양의 나노세공 혹은 나노채널이 규칙적으로 배열되어, 높은 내부 표면적을 갖는 특징과 함께, 높은 비율로 분산된 금속 성분 등 뛰어난 물리화학적 특성으로 인해 활발한 연구가 이뤄지고 있는 물질이다. 특히, 빈 배위결합 자리(Open coordination sites)를 가지는 금속 유기 구조체의 경우, 가스 분리, 가스 흡착 및 촉매 등 다양한 응용 분야에 잠재성을 가지고 있는 물질로서 현재 활발히 연구되고 있다. 하지만, 이러한 공정 분야에 응용하기 위해서는 반드시, 빈 결합 자리에 결합되어 있는 용매 분자를 제거하는 활성화 공정이 선행되어야 한다. 현재까지 열과 함께 진공을 이용하여 수행되는 열적 활성화(Thermal Activation)가 유일한 방법으로 이용되고 있다.

본 연구에서는 열적 활성화 방법이 아닌, 화학적인 경로로서 메틸렌 클로라이드(MC) 자체만으로 빈 배위 결합 자리를 화학적 활성화(Chemical Activation)하는 연구를 진행하였다. 메틸렌 클로라이드는 일반적으로 열적 활성화의 전처리 단계로서 사용되고 있지만, 그 자체만으로 빈 배위결합 자리 활성화를 수행할 수 있는 물질로서 알려진 바가 없다. 뿐만 아니라, 금속 유기 구조체의 빈 배위결합 자리와 메틸렌클로라이드와의 배위 결합에 대한 화학적 메커니즘에 대해 정확하게 규명되지 않았다. 본 연구에서, 라만 연구를 기초로 하여 금속 유기 구조체의 빈 배위결합 자리에서 메틸렌 클로라이드가 용매 분자를 탈배위하는 화학적 활성화의 기능을 밝혀내고, 그에 대한 화학적/물리적 메커니즘을 제안하였다. 또한, 금속 유기 구조체인 HKUST-1 Film을 통해서, 제안된 방법이 넓은 면적의 금속 유기 구조체 Film의 빈 배위결합 자리 활성화에 매우 적합하며, 빠르고 용이한 화학적 활성화임을 입증하였다.

Keywords: 금속 유기 구조체, 빈 배위결합 자리(Open coordination sites), 메틸렌클로라이드(MC), 활성화(Activation)